Multicomponent Vapor–Liquid Equilibrium Measurement and Modeling of Ethylene Glycol, Water, and Natural Gas Mixtures at 6 and 12.5 MPa

Kruger, Francois J.; Kontogeorgis, Georgios M.; Solbraa, Even; von Solms, Nicolas

Published in:
Journal of Chemical and Engineering Data

Link to article, DOI:
10.1021/acs.jced.8b00495

Publication date:
2018

Document Version
Peer reviewed version

Multi-component vapor-liquid equilibrium measurement and modeling of ethylene glycol, water and natural gas mixtures at 6 and 12.5 MPa

Francois J. Kruger[‡], Georgios M. Kontogeorgis[‡], Even Solbraa[†], Nicolas von Solms[‡,]*

‡ Department of Chemical and Biochemical Engineering, Center for Energy Resources Engineering (CERE), Technical University of Denmark, DK-2800, Lyngby, Denmark

† Equinor (formerly Statoil ASA), Research and Development Center, N-7005, Trondheim, Norway

ABSTRACT

High pressure subsea natural gas dehydration (NGD) units using ethylene glycol (MEG) absorption have been proposed. To expand the experimental database and assist design qualification, new VLE experimental data have been measured for a 20-component glycol-water-natural gas mixture at T = (288-323) K, p = (6.0, 12.5) MPa and $w_{MEG,feed}$ = (90, >99.8) %. MEG, H_2O, CO_2, N_2 and alkane (methane to *n*- and *i*-pentane) phase distributions have been quantified. Experimental uncertainty ranges from ±2-42%, with the greatest uncertainty for the quantification of trace components. Experimental results are modeled using the Cubic-Plus-Association (CPA) equation of state. Over-predictions (~9%) are observed for the water content of the vapor phase. CO_2 is shown to have a large effect on y_{MEG}, leading to modeling deviations in the order of 65%. Relatively accurate prediction of the natural gas partition coefficients was observed for major components C_1-C_3 and CO_2, with modeling errors ranging from 5% for methane to 10% for CO_2. More significant deviations were observed for trace components, with the largest deviation of 73% N_2. The CPA model provides both satisfactory and conservative results suitable for use in NGD process designs. Based on this work, operation at subsea conditions would significantly improve dehydration capability.

INTRODUCTION

Water contamination in natural gas pipelines can result in the formation of gas hydrates or, when combined with other natural gas components such CO_2 and H_2S, leads to corrosion.[1] This presents significant risks in downstream facilities and transport networks in terms of flow assurance and asset integrity. Although several other options exist for natural gas dehydration (e.g. membrane separation[2–4], molecular sieves[5–7], absorption into ionic liquids[8], supersonic nozzles[9] and isenthalpic gas cooling[10,11]), glycol absorption is by far the most used method for industrial applications.[12]

Meanwhile recent technical advances have seen an increase in subsea processing installations, which present several advantages over onshore processing. One such proposal[13] considers natural gas dehydration at the seabed. Due to the proximity to the reservoir, water may be absorbed into either mono- (MEG) or tri-ethylene glycol (TEG) at processing pressures above 10 MPa. Performing equipment sizing and absorbent selection for process designs and feasibility studies of such facilities, requires accurate thermodynamic models. The development and evaluation of such models requires a wide range of reliable equilibrium data.

In this work we focus on the application of MEG for subsea natural gas dehydration, for which the open literature contains relatively few data. Gas solubility measurements in binary mixtures of MEG with methane (C_1), ethane (C_2), nitrogen (N_2) and carbon dioxide (CO_2) have been published.[14–20] Ternary data for MEG-H_2O-C_1 have also been published[16,18,21], while MEG-H_2O-C_1-CO_2/C_3 were measured by the Gas Processors' Association.[22] In general, the available ternary and multicomponent data have been measured using lower MEG feed concentrations (~ 50-60 wt% aqueous), which are more applicable to hydrate inhibition studies.

Cubic equations of state such as Soave-Redlich-Kwong (SRK)[23] and Peng-Robinson (PR)[24] have a long history of application in the oil & gas industry and form the basis of many other models. For their application in natural gas dehydration, these models often fall short due to not accounting for specific molecular interactions such hydrogen bonding. The Statistical Associating Fluid Theory (SAFT)[25–27] models were developed in the late 1980s and contain a term which specifically accounts for hydrogen bonding (also called association). In the development of the Cubic-Plus-Association (CPA)[28] model, this association term was combined with SRK. The resultant model remains relatively simple while expressly accounting for hydrogen bonding. As such, CPA is ideally suited for the description of the natural gas dehydration where alkanes (for which SRK was developed) interact with water and glycols (which hydrogen bond). CPA has been used in several studies for relevant systems, where the requirements for new data are also highlighted.[18,21,29–30]

In this work we present the results of vapor-liquid equilibrium (VLE) experiments for MEG (90 wt% aqueous and pure) with a natural gas mixture. The experimental conditions were varied with temperature and pressure within the following ranges: T = (288 – 323) K, p = (6.0, 12.5) MPa. Additionally, the newly measured data was used in the evaluation of CPA in order to assess its applicability for design of natural gas dehydration facilities. For such designs, it is important to understand both the accuracy and nature of the deviation of the models. Critical process parameters include product specifications (e.g. the amount of water and glycol in the vapor phase) and the amount of dissolved natural gas, which must to be accounted for in the glycol regeneration unit.

EXPERIMENTAL METHOD

APPARATUS

The experiments were conducted using an apparatus manufactured by Sanchez Technology (now Core Laboratories), which has been described previously.[21] For the quantification of natural gas compounds, a micro gas chromatograph (μGC) was added to the experimental setup. An updated schematic of the equipment is presented in Figure 1.

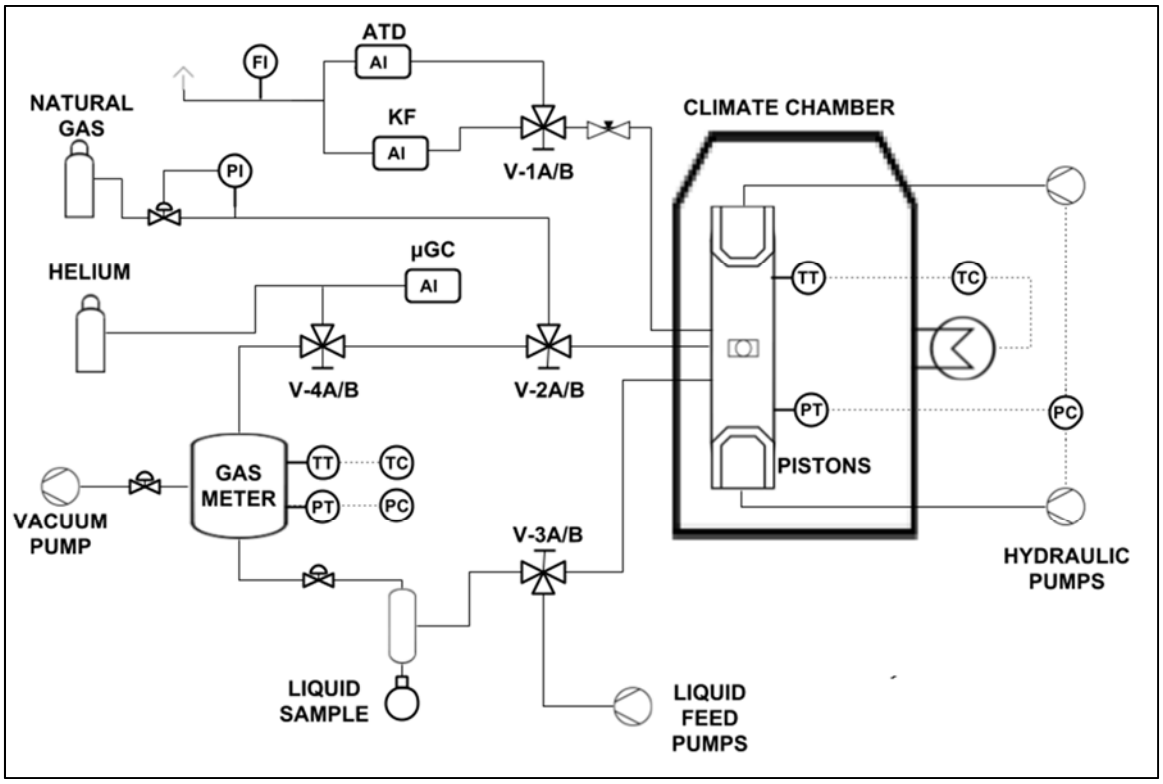

Figure 1. Simplified schematic of the high-pressure equilibrium cell and sampling pathways.

The loading and equilibration procedures were unchanged from Kruger et al.[21] with the exception that pure methane has been replaced by a natural gas mixture. The following measurements were made during each experiment:

1. 4-6 vapor phase samples from the cell to the μGC via V-2A/B and V-4A/B to analyze for natural gas component (y_{NG})

2. Liquid sample (± 25 mL) via V-3A/B, from which 'flash gas' is collected in the gasmeter
    a. Sample mass
    b. Karl Fischer (KF) water content analysis (min. 2 repeated measurements)
    c. Density measurements (min. 2 repeated measurements)
3. Analysis of the 'flash gas' (x_{NG}) from the gasmeter to the μGC (~ 5-8 samples)
4. KF analysis of the vapor phase (y_{H2O}): 5-8 samples (min. 2 flushes) of ~ 0.5 L, as measured by the gas flow meter (FI in the Figure 1) via V-1A/B
5. MEG in vapor phase (y_{MEG}): 10 samples [V = (0.1 – 0.5) L] adsorbed onto Tenax® tubes (ATD in Figure 1) via V-1A/B

y_{MEG} was quantified using an Agilent 5975C GC-MS (Varian CP7448 capillary column). Duplicate three-point calibration (versus standard solutions) was performed for each batch of samples. The natural gas components were analyzed using an Agilent 3000 μGC, with four channels, each fitted with a TCD detector. The column details are provided in Table 1. The μGC was calibrated using four calibration gases, allowing for the quantification of up to 15 components. Periodic verification and re-calibration were performed in order to ensure accurate measurements.

Table 1. Column details [ID = inner diameter, L = length, C_i = Alkane of carbon chain-length i] for each of the four channels in the Agilent 3000 μGC

Channel	Pre-column (*Film*/μm, *ID*/μm, *L*/m)	Column (*Film*/μm, *ID*/μm, *L*/m)	Components
A	PLOTU 30/320/3	Molsieve 12/320/10	O_2, N_2, C_1
B	PLOTQ 10/320/1	PLOTU 30/320/8	CO_2, C_1
C	Alumina 3/320/1	Alumina 8/320/10	C_3, nC_4, iC_4
D	-	OV1 1.2/150/8	nC_5, iC_5, nC_6, Benzene, nC_7, nC_8, nC_9

Quantification of the total dissolved natural gas (x_{NG}) was done using the same equations as Kruger et al.[21] for C_1. The dissolved content of each component was quantified using the 'flash gas' composition measurements of the μGC. For all μGC measurements, air ingress into the sampling pathways could not be completely negated. Therefore the first few samples were used to flush the sampling system until a predefined threshold (i.e. GC peak area) for O_2 content was met. Thereafter it was still necessary to reprocess the N_2 composition, by subtracting the amount of air contamination. It was assumed that the N_2 contamination from air was related to the O_2 content according to a 79:21 ratio. Leakage was typically negligible for the y_{NG} measurements (due to the high pressure in the system after a single sample flush), while for the contamination of the 'flash gas' was typically around 1.5 mol%.

During sampling, the pressure in the cell was maintained by manipulating the relevant hydraulic piston. Instantaneous pressure fluctuations (resulting from the opening of a sampling valve) of greater than 0.8% of the experimental pressure would result in automatic exclusion of the results, but typically values better than 0.33% were observed.

A summary of all the analytical equipment is provided in Table 2.

Table 2. Overview of experimental apparatus for compositional analyses [NG = natural gas components, (v) = vapor phase, (l) = liquid phase, CD = calibration deviation, u = uncertainty]. Additional information in the Supporting Information (see Tables S1-S2)

Measurement	Label in Figure 1	Equipment Type	Description	CD / uncertainty
H_2O (v)	AI: KF via V-1A/B	KF Coulometer	Metrohm 831	$u(y_{H2O}) = \pm 3\%$
MEG (v)	AI: ATD via V-1A/B	ATD tubes + GC-MS	Tenax® TA (Perkin Elmer) + Agilent 5975C	$u(y_{MEG}) = \pm 12\%$
Flow rate (v)	FI	Drum-type gas meter	Ritter TG 1/5	CD = 0.09%
Density (l)	Liquid Sample	Densometer	Anton Paar DMA 4500M	$u(\rho) = \pm 0.00007$ $g \cdot mol^{-1}$
H_2O (l)	Liquid Sample	KF Volumetric	Metrohm 915 KF Ti-Touch	$u(x_2) = \pm 2\%$
Mass	Liquid Sample	Scale	Ohaus Explorer Pro	$u(m) = \pm 0.001$ g
NG (l)	Liquid sample to µGC via Gasmeter	GC	Agilent 3000 µGC (4 channels, TCD)	Concentration dependent. See Table S1
NG (v)	µGC via V-2A/B and V-4A/B	GC	Agilent 3000 µGC (4 channels, TCD)	Concentration dependent. See Table S2

MATERIALS

A total of 20 compounds were used in this work. The compounds were classified as a liquid or gas depending on how they were loaded into the equilibrium cell. Prepared MEG-H_2O mixtures were loaded into the cell using high pressure Quizix pumps. The specifications of the liquid compounds are given in Table 3.

Table 3. Material specifications for the liquid components used in this study

No.	Name	CAS No.	Supplier	Purity	Water content	Additional purification
1	MEG	107-21-1	Sigma-Aldrich (324558)	99.8 mol%	< 0.003% (by KF)	None
2	Water (H_2O)	7732-18-5	ELIX® Reference 5	Resistivity @ 298.15 K: 10-15 μS/cm	N/A	None

The other 18 compounds were loaded into the cell from a natural gas cylinder via valve V-2A/B. The gas composition was determined by GC with the molar composition given in Table 4. The gas phase content for components 12-20 were in the low ppm level. For practical purposes, these trace components were too near the limit of detection of the μGC to allow for accurate quantification, especially for the 'flash gas' analysis.

Table 4. Molar composition, as determined by GC, for natural gas mixture used in this study (DM = di-methyl, M = methyl, cy = cyclo)

No.	Name	CAS No.	*MW* $g \cdot mol^{-1}$	*Molar Composition* %	*Subscript*
3	Nitrogen	7727-37-9	28.01	0.899	N_2
4	Carbon Dioxide	124-38-9	44.01	2.517	CO_2
5	Methane	74-82-8	16.04	91.74	C_1
6	Ethane	74-84-0	30.07	4.265	C_2
7	Propane	74-98-6	44.10	0.5025	C_3
8	*i*-Butane	75-28-5	58.12	0.0474	iC_4
9	*n*-Butane	106-97-8	58.12	0.0192	nC_4
10	*i*-Pentane	78-78-4	72.15	$3.50 \cdot 10^{-3}$	iC_5
11	*n*-Pentane	109-66-0	72.15	$2.80 \cdot 10^{-3}$	nC_5
12	2,2-DM-Propane	463-82-1	72.15	$8.00 \cdot 10^{-5}$	$22DMC_3$
13	2,2-DM-Butane	75-83-2	86.18	$5.00 \cdot 10^{-5}$	$22DMC_4$
14	cy-Pentane	287-92-3	70.13	$1.50 \cdot 10^{-4}$	cC_5
15	2,3-DM-Butane	79-29-8	86.18	$8.00 \cdot 10^{-5}$	$23DMC_4$
16	2-M- Pentane	107-83-5	86.18	$4.10 \cdot 10^{-4}$	$2MC_5$
17	3-M- Pentane	96-14-0	86.18	$2.30 \cdot 10^{-4}$	$3MC_5$
18	*n*-Hexane	110-54-3	86.18	$5.70 \cdot 10^{-4}$	nC_6
19	Heptanes total	-	100.20	$1.60 \cdot 10^{-3}$	nC_7
20	Octanes total	-	114.23	$6.50 \cdot 10^{-4}$	nC_8

EXPERIMENTAL MATRIX

11 different experimental conditions were selected with each experiment repeated once. The majority of the experiments were performed using an aqueous MEG solution (90 wt%) at two selected pressures (6.0, 12.5 MPa). A summary of the experimental matrix is provided in Table 5.

Table 5. Temperature, pressure and gas/liquid loading volumes for each experiment in this study

exp. no.	T / K	p / MPa	w_{MEG} / g·g^{-1}	V_{liquid} /mL	V_{gas} / mL
1	288.18	6.02	0.9	60.1	271
2	293.19	6.00	0.9	60.2	264
3	298.15	6.00	0.9	60.8	266
4	303.16	6.00	0.9	60.4	268
5	313.18	5.99	0.9	60.2	274
6	323.17	6.00	0.9	60.2	243
7	303.16	12.51	0.9	60.8	198
8	313.18	12.49	0.9	60.2	152
9	323.17	12.49	0.9	60.2	158
10	303.17	6.00	>0.998	60.6	265
11	303.18	12.50	>0.998	60.7	144

For VLE flash calculations, the overall composition can determined by adding the vapor and liquid molar quantities. The vapor molar quantity is calculated by combining the compositions from Table 4 with the relevant T, p and V_{gas} from Table 5 and the compressibility factor. The compressibility factor should be calculated using a suitable equation of state e.g. CPA.

THERMODYNAMIC MODELING

CUBIC-PLUS-ASSOCIATION EQUATION OF STATE

CPA[28] (see Eqs. 1-3) was developed as a hybrid of the widely used cubic equations of state (specifically SRK) and the SAFT models. Its relative simplicity while simultaneously accounting for association, means that CPA is ideally suited for modeling glycol-water-natural gas systems. In this work we have used the 1999 version of CPA[31], which has a simplified radial distribution (g). Several excellent reviews of this model are available in the literature.[32–36]

$$p = p_{SRK} + p_{assoc}$$

$$= \frac{RT}{V_m - b} - \frac{a_0\left[1 + c_1\left(1 - \sqrt{T_R}\right)\right]^2}{V_m(V_m + b)} - \frac{RT}{2V_m}\left(1 + \rho_m \frac{\partial \ln g}{\partial \rho_m}\right)\sum_i x_i \sum_{A_i}\left(1 - X_{A_i}\right)$$

Eq. 1

$$X_{A_i} = \frac{1}{1 + \rho \sum_j x_j \sum_{B_j}\left(X_{B_j}\, \Delta^{A_i B_j}\right)}$$

Eq. 2

$$\Delta^{A_i B_j} = g(\rho)\left[\exp\left(\frac{\varepsilon^{A_i B_j}}{RT}\right) - 1\right] b_{ij} \beta^{A_i B_j}$$

Eq. 3

In the above equations, p, R, T, V_m, T_R, ρ and x refer to the pressure, universal gas constant, temperature, molar volume, reduced temperature, molar density and mole fraction respectively. X_{Ai} is defined as the fraction of nonbonded sites for association site A on molecule i and Δ^{AiBj} is defined by the association interaction between site A on molecule i and site B on molecule j.

For non-associating compounds, three pure component parameters are required:

- Molecular co-volume (b) [$cm^3 \cdot mol^{-1}$]
- Attractive energy parameter (a_0), often presented in the form $\Gamma = a_0/(b \cdot R)$ [K]
- Dimensionless temperature correction (c_1)

For associating compounds, two additional pure component parameters are defined:

- Association energy (ε), shown here in the reduced for ε/R [K]
- Association volume (β)

For associating compounds, it is also necessary to define an association scheme. MEG and H_2O are usually defined according to the 4C scheme, which consists of two positive (electron donor) and two negative (electron acceptor) association sites. More recently, the 4F association scheme, which consists of two binary (which can accept or donate an electron) and two negative association sites, has been proposed for MEG.[37]

In the literature, natural gas components from this study are typically modeled as non-associating compounds. For the components in this study, CO_2 is the only exception as it is often modelled as a cross-associating (solvating) compound. Due to its complex interactions in mixtures, several different methodologies have been tested for CO_2. One approach considers different association configurations i.e. non-associating, solvation and self-association.[38–43] Other studies[44,46] have considered the incorporation of additional model terms to account for polar and quadrupolar interactions. In the present study we considered only the non-associating and solvation approaches. It was found that the best results for CO_2 were obtained when modeled it as a solvating compound with 1 negative (electron acceptor) association site.

PURE COMPONENT PARAMETERS

Table 6. Pure component parameters, with Γ = a0/(b·R), for the CPA EoS from literature.[31,38,39,46–48]

	T_C / K	b_0 / $cm^3 \cdot mol^{-1}$	Γ / K	c_1	ε/R / K	$\beta \cdot 10^3$	Scheme
MEG	720.0	51.4	2531.71	0.6744	2375.752	14.1	4C
H_2O	647.3	14.515	1018.39	0.67359	2003.25	69.2	4C
N_2	126.2	26.05	634.07	0.49855	-	-	-
CO_2	304.2	27.20	1551.22	0.76020	-	-	0ed-1ea
C_1	190.6	29.10	959.03	0.44718	-	-	-
C_2	305.3	42.90	1544.55	0.58463	-	-	-
C_3	369.8	57.83	1896.45	0.63070	-	-	-
iC_4	407.8	74.70	2078.62	0.70210	-	-	-
nC_4	425.1	72.08	2193.08	0.70771	-	-	-
nC_5	469.7	91.01	2405.11	0.79858	-	-	-
$2MC_5$	497.7	90.40	2823.00	0.75610	-	-	-
$3MC_5$	504.6	106.31	2607.08	0.79961	-	-	-
nC_6	507.6	107.89	2640.03	0.83130	-	-	-
nC_7	540.2	125.35	2799.76	0.91370	-	-	-
nC_8	568.7	142.44	2944.91	0.99415	-	-	-

ed, electron donor; ea, electron acceptor

The literature pure component parameters used in this work are shown in Table 6. For 5 of the natural gas components, no literature parameters could not be found. In order to regress new parameter sets, we incorporated the bootstrap method and uncertainty analysis.[37, 45] Pure component vapor pressure and saturated liquid density correlations from the DIPPR Database[49] were used in the minimization routine and 1000 bootstrap steps were done for each parameter set. The objective function is shown in Eq. 4. The new parameters are presented in Table 7, along with the 95% confidence intervals for the vapor pressure and density errors.

$$OF_{min} = \sum_{n} \left[\left(\frac{p_{i,sat}^{DIPPR} - p_{i,sat}^{CPA}}{p_{i,sat}^{DIPPR}} \right)^2 + \left(\frac{\rho_{i,sat}^{DIPPR} - \rho_{i,sat}^{CPA}}{\rho_{i,sat}^{DIPPR}} \right)^2 \right]$$

Eq. 4

Table 7. Bootstrapped parameters for 22DMC$_3$, iC$_5$, 22DMC$_4$, cC$_5$ and 23DMC$_4$ by regression versus DIPPR correlations for saturated vapor pressure (p_{sat}) and density (ρ_{sat}) for T_R = (0.4-0.9).

	T_C / K	b_0 / cm^3·mol^{-1}	Γ / K	c_1	*AARD / %* p_{sat}	*AARD / %* ρ_{sat}
22DMC$_3$	433.8	92.05	2202.32	0.72389	0.32-0.95	0.70-1.0
*i*C$_5$	460.4	90.70	2349.51	0.76425	0.24-0.45	0.95-1.1
22DMC$_4$	489.0	107.42	2439.72	0.82778	1.5-2.3	0.035-0.052
cC$_5$	511.7	76.40	2588.97	0.73946	0.67-1.4	1.0-1.5
23DMC$_4$	500.0	106.42	2541.43	0.80511	0.36-0.51	0.27-0.61

EXTENSIONS TO MIXTURES

For mixtures, mixing and combining rules are also required. Conventional mixing rules (see Eqs. 5 & 6) are used in this work. A total of 16 binary interaction parameters ($k_{ij}(T)$ in Eq. 5) have been used in this study and these are presented in Table 8.

$$a(T) = \sum_i \sum_j x_i x_j a_{ij}(T) \;\; with \;\; a_{ij}(T) = \sqrt{a_i(T) \cdot a_j(T)} \left(1 - k_{ij}(T)\right)$$

Eq. 5

$$b = \sum_i x_i b_i$$

Eq. 6

For the cross-association between MEG and H_2O, Elliot's combining rule (ECR) (see Eq. 7) has been recommended in the literature.[18,32,33]

$$\Delta^{A_iB_j} = \sqrt{\Delta^{A_iB_i}\Delta^{A_jB_j}}$$

Eq. 7

Conversely, the cross-association of CO_2 with MEG/H_2O is modeled using the modified CR-1 rule (mCR1)[50] for which the cross-association parameters ($\varepsilon^{cross} = \varepsilon^{AiBj}$, and $\beta^{cross} = \beta^{AiBj}$ in Eq. 3, with b_{ij} given as $(b_i+b_j)/2$) must be defined. The following parameters from Tsivintzelis et al.[39,43,51] have been used.

- CO_2-MEG: $\beta^{cross} = 0.1274$ with $\varepsilon^{cross}/R = 0.5 \cdot \varepsilon^{MEG}/R$
- CO_2-H_2O: $\beta^{cross} = 0.0164$ with $\varepsilon^{cross}/R = 1707.96$ K

In the first case, the traditional approach is taken where the cross-association energy parameter is set to half the value of the self-associating component. In the second case, the cross-association energy was based on experimental data for weak Lewis acid-base interactions. In both cases the β^{cross} and k_{ij} parameters (presented in Table 8) were simultaneously regressed against experimental phase equilibrium data.

Table 8. Binary interaction parameters for the CPA EoS found in the literature[30,37,39,43,51–53], implemented in Eq. 5 as $k_{ij}(T) = k_{ij,a} + k_{ij,b} \cdot T + k_{ij,c}/T$.

No.	Comp 1	Comp 2	$k_{ij,a}$	$k_{ij,b}$	$k_{ij,c}$
1	MEG	H_2O	-0.1284	-	-
2	MEG	CO_2	0.2253	-	-
3	H_2O	CO_2	0.00460	0.000331	-
4	MEG	C_1	0.1786	-	-
5	H_2O	C_1	0.7988	-	-236.5
6	MEG	C_2	0.1451	-	-
7	H_2O	C_2	0.54729	-	-143.25
8	MEG	C_3	0.11324	-	-
9	H_2O	C_3	0.1135	-	-
10	MEG	nC_4	0.06975	-	-
11	H_2O	nC_4	0.0875	-	-
12	MEG	iC_4	0.0209	-	-
13	MEG	nC_5	0.035	-	-
14	H_2O	nC_5	0.0615	-	-
15	MEG	nC_6	0.031	-	-
16	H_2O	nC_6	0.0355	-	-

Very few data are available for VLE measurements of natural gas in aqueous glycol where all components in both phases are quantified. In general there are more binary data available where the liquid phase (i.e. fraction of dissolved gasses) has been quantified. k_{ij} parameters which have been fitted to binary phase equilibrium data can be used predictively in multicomponent mixtures. In this study we have found that CPA performance for dissolved gasses is most sensitive to the $k_{MEG\text{-}gas}$ as opposed to $k_{H2O\text{-}gas}$.

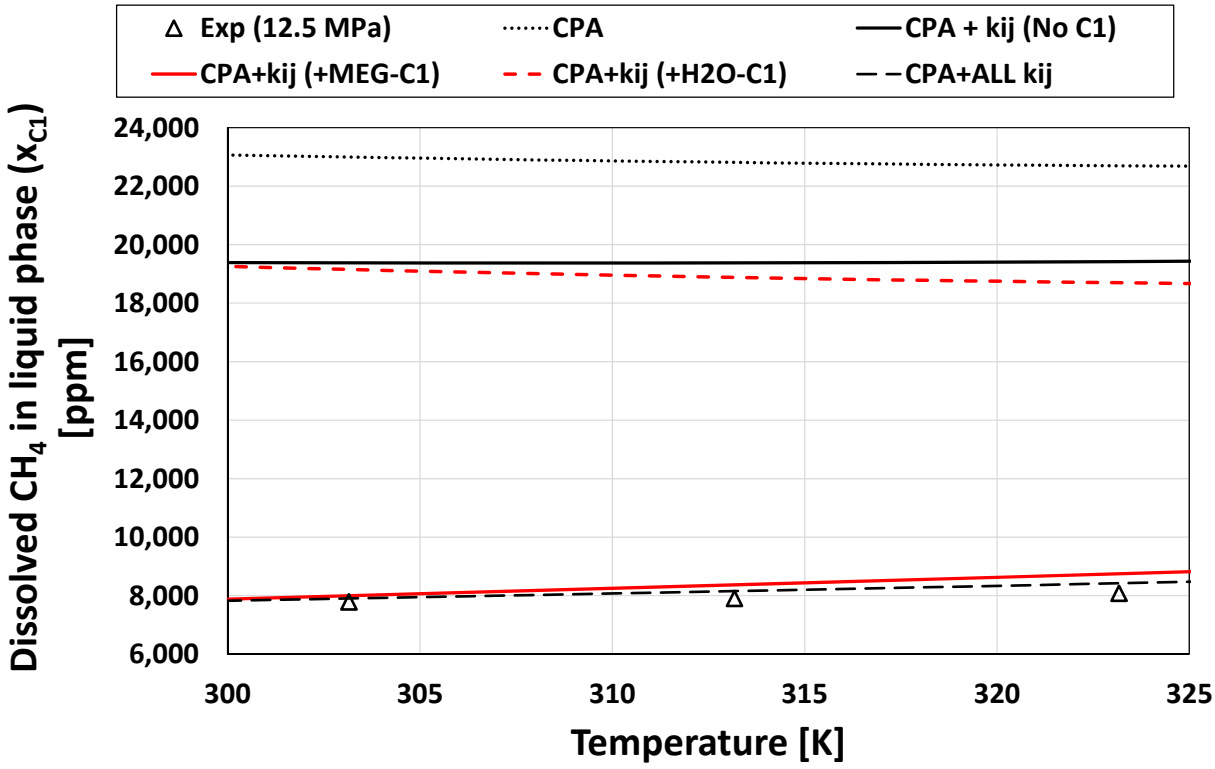

Figure 2. Effect of binary interaction parameters for the CPA model predictions of experimental liquid phase solution of methane (x_{C1}) at T = (303-323) K, p = 12.5 MPa and MEG feed purity of w_{MEG} = 90%.

This effect is demonstrated for x_{C1} in Figure 2, where interaction parameters are sequentially added to CPA to demonstrate the improvement in modeling performance. The top-most line (dotted black) represents CPA without any k_{ij} and the modeling error versus the three experimental data points is calculated as 187%. The 2nd line (solid black) represents the CPA prediction using 14 of the 16 parameters from Table 8. Only $k_{MEG\text{-}C1}$ and $k_{H2O\text{-}C1}$ have been excluded and the model performance improves to a 144% over-prediction. For the next line (dashed red), $k_{H2O\text{-}C1}$ is also included (i.e. 15 of 16 parameters from Table 8) and error improves slightly to 138%. For the case where $k_{MEG\text{-}C1}$ is used instead of $k_{H2O\text{-}C1}$ (solid red), the CPA performance improves to 5%. Finally all 16 parameters are included (dashed black) such that an overall error of 3% is achieved. Figure 2 is representative of the magnitude of the

performance effect for all dissolved hydrocarbons measured in this study. Although the largest improvement is due to k_{MEG-C1}, the contribution of k_{H2O-C1} should not be neglected due to its effect (in combination with k_{MEG-C1}) on the temperature-dependency for x_{C1} in the mixture. It was not investigated whether the magnitude of the improvement is solely due to the relative concentration of MEG and H_2O in the studied mixtures or is an inherent property of the CPA model and the MEG/H_2O parameter sets.

Due to the importance of MEG-gas interactions, every effort was made to find suitable interaction parameters. A new k_{ij} was regressed for MEG-*i*C_4 against the only available literature phase equilibrium data (a single Henry's constant data point[54]). The same methodology has been applied in the literature[51] for MEG-*n*C_4.

For binary systems containing H_2O, there is significantly more data available. Liang et al.[30] developed temperature dependent binary interaction correlations for H_2O-C_1/C_2/C_3/*n*C_4 binary systems over a wide range of temperature and pressure, although modeling difficulties were reported for C_2 and up. In our previous work[21] we showed that CPA over-predicts the dissolved methane content in MEG-H_2O-C_1 and similar results were achieved by Boesen et al.[29] The magnitude of this over-prediction can be improved to approximately 5% through the use of more appropriate k_{ij} parameters.

A third important class of binary interaction parameters was identified for interactions involving CO_2, especially those with MEG/H_2O. Interaction parameters have been published[39] for CO_2-C_1/C_2/C_3/*n*C_4, but these negatively affected the model performance. Similarly for MEG-N_2, a temperature dependent k_{ij} correlation was regressed against data from Zheng et al.[15], but did not improve the model performance.

RESULTS & DISCUSSION

EXPERIMENTAL DATA

The experimental results are presented in Tables 9 (y_{MEG}, y_{H2O}, x_{NG}) and 10 (partition coefficients for the gas components). The relative standard deviations are provided in the Supporting Information (see Tables S1 and S2). Each reported value represents the average of the two experiments, as per the conditions listed in Table 5.

Unless stated otherwise, we present uncertainty in the relative form

$$u_{r,x} = \frac{CI \cdot \sigma_x}{|\mu_x|} \cdot 100\ [\%]$$

Eq. 8

In Eq. 8, σ_x refers to the standard deviation of the experimental, μ_x is the average value or experimental result and *CI* refers to the confidence interval multiplier. For confidence intervals of 0.683, 0.954 and 0.997, CI has values of 1, 2 and 3 respectively.

Model performance is evaluated according to average absolute relative deviation

$$AARD = \frac{1}{n}\sum \left| \frac{value_{model} - value_{exp}}{value_{exp}} \right| \cdot 100\ [\%]$$

Eq. 9

In Table 9, the results for y_{MEG} at high temperatures are not shown due to the same experimental difficulties described previously.[21] From Table S1 it can be seen that the uncertainty generally increases as concentration decreases, with C_1-C_3 and CO_2 having the highest degree of certainty while the values for MEG, N_2, nC_5 and iC_5 are the most uncertain. The relative uncertainty of the data ranges from 3% for C_1 to 42% for iC_5.

Table 9. Experimental results for MEG and H_2O in the vapor phase, and dissolved natural gas components at Temperature T and Pressure p. Standard uncertainties u are u(T) = 0.05 K and u(p) = 2·10-3p. Relative standard deviations for composition data are reported in Table S1.

exp. no.	T K	p MPa	y_{MEG} ppm	y_{H2O} ppm	x_{CO2} ppm	x_{N2} ppm	x_{C1} ppm	x_{C2} ppm	x_{C3} ppm	x_{nC4} ppm	x_{iC4} ppm	x_{nC5} ppm	x_{iC5} ppm
1	288.2	6.0	0.69	91.1	1375	23	4490	479	67	5.9	3.5	0.6	0.8
2	293.2	6.0	0.95	116	1254	18	4423	464	65	5.6	3.2	0.6	1.3
3	298.2	6.0	1.2	152	1148	40	4322	436	59	4.9	2.9	0.5	0.9
4	303.2	6.0	2.9	195	1081	40	4386	425	56	4.5	2.6	0.5	0.8
5	313.2	6.0	13.6	318	1032	133	4418	412	55	4.7	2.4	0.6	0.6
6	323.2	6.0	-	510	857	111	4397	391	51	3.9	2.4	0.4	0.5
7	303.2	12.5	5.9	127	1938	43	7813	616	70	5.1	3.1	0.4	0.9
8	313.2	12.5	15.0	193	1664	67	7930	605	70	5.0	3.0	0.4	0.6
9	323.2	12.5	-	309	1558	73	8107	611	71	5.2	3.2	0.5	0.6
10	303.2	6.0	3.9	16.4	1546	77	6722	761	116	10.8	6.6	1.0	1.4
11	303.2	12.5	8.4	13.0	2601	78	12313	1085	140	11.0	6.8	1.0	1.2

Results for *n*-hexane (nC_6) are not presented as the liquid phase content, being too near the limits of detection of μGC, could not be reliably detected and measured. Similar trends w.r.t. uncertainty vs. concentration are observed for the experimental uncertainty of the data (see Table S2) presented in Table 10. The relative uncertainty ranges between 3% and 39%. Data for C_1 are most certain, while experimental values for the C_5 alkanes are shown to be the least certain.

Table 10. Experimental partition coefficients (y_i/x_i) for natural gas components. Standard uncertainties u are u(T) = 0.05 K and u(p) = 2·10-3p. Relative standard deviations for composition data are reported in Table S2.

exp. no.	T / K	p / MPa	CO_2	N_2	C_1	C_2	C_3	nC_4	iC_4	nC_5	iC_5
1	288.2	6.0	16.1	402	205	89.0	76.2	61.4	79.3	46.5	46.3
2	293.2	6.0	17.7	508	208	91.9	78.6	63.7	87.9	43.2	29.7
3	298.2	6.0	19.4	239	213	97.9	86.2	73.5	97.8	49.4	44.9
4	303.2	6.0	20.8	233	210	101	90.8	80.0	110	57.4	49.3
5	313.2	6.0	21.7	72.2	208	102	93.1	77.8	118	45.0	64.3
6	323.2	6.0	26.4	85.8	209	108	101	92.2	115	62.1	68.4
7	303.2	12.5	11.8	219	118	69.9	73.7	72.2	91.1	67.2	42.6
8	313.2	12.5	13.1	141	116	69.9	73.8	73.1	93.0	71.8	59.5
9	323.2	12.5	14.3	130	113	69.6	72.0	70.1	89.3	58.3	60.7
10	303.2	6.0	14.1	123	137	55.2	43.4	32.3	41.9	25.6	23.7
11	303.2	12.5	8.2	121	74.8	39.0	36.5	32.5	41.4	27.0	29.6

For the evaluation of the data it is useful to consider the following:

- Temperature effects are shown by comparison of values within exp. 1-6, and 7-9
- Pressure effects can be seen by comparison of exp. 4-6 with 7-9, and 10 with 11
- The effect of MEG purity is seen by comparing exp. 4 with 10, and 7 with 11

It is important to understand its influence operational variables (T, p and MEG purity) on the following design variables:

- The amount of water in vapor phase (product stream)
- The amount of MEG lost to the vapor phase (product stream)
- The amount of natural gas lost to the liquid phase (regeneration stream)
- The effect of inert gasses such as CO_2 and N_2

Each of these factors can have an impact on the design in terms of product quality, recycle rate, regeneration and optimal operating point.

An outcome of this work was to determine whether the trends predicted by the CPA are accurate for multicomponent mixtures applicable to natural gas dehydration. The CPA equation of state was used to predict the experimental data, using the parameters and interaction parameters given in Tables 6-8. For accurate determination of the mass of gas loaded into the cell, the compressibility factor was also calculated. Although results for the full 20-component system are shown here, we also performed modeling with fewer components and suitable grouping methods. Negligible differences in modeling results were observed for the components which were experimentally quantified in both phases. For the modeling of experiments 10 and 11, it was assumed that the H_2O content of the liquid is 99.8 mol% as per the supplier specification in Table 3.

DISCUSSION: MEG & WATER PRESENT IN THE VAPOR PHASE

In the evaluation of the data and modeling with respect to natural gas dehydration, the starting point is the water content of the vapor phase i.e. the product stream. The water in gas (y_{H2O}) results for experiments 1-9 and CPA modeling are shown in Figure 3.

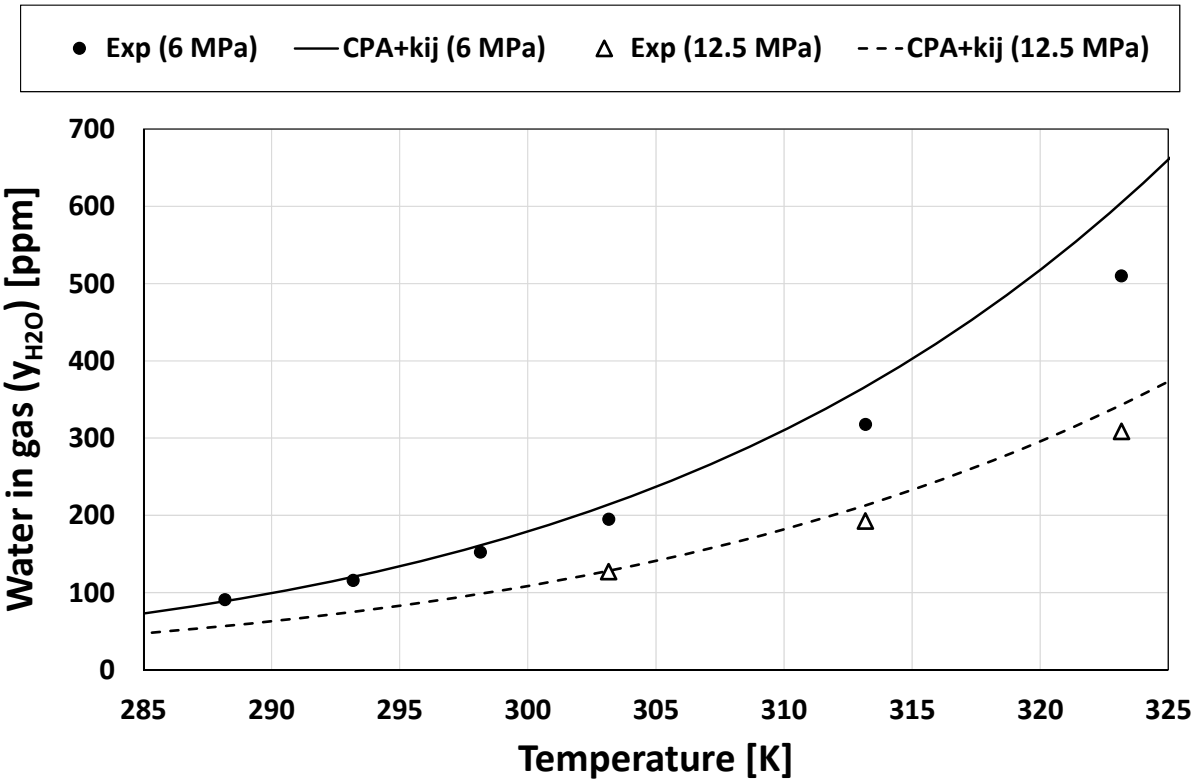

Figure 3. Experimental vapor phase water content (y_{H2O}) in a mixture with MEG and natural gas components at T = (288-323) K and p = (6, 12.5) MPa.

The water vapor content exhibits the expected exponential increase with temperature with values ranging between 100 and 500 ppm. An increase in pressure from 6.0 to 12.5 MPa results in an approximately 30% lower water vapor content. The average experimental uncertainty was calculated as ± 2%. Here the measured values for experiments 10 and 11 are not taken into account as there should be little to no water in the system. It is noted that the experimental values presented in Figure 3 are similar (especially at lower temperatures T <

300 K) to the equivalent experiments using pure methane[21] rather than a natural gas mixture. It is therefore implied that the additional natural gas components have a relatively minor effect on the dehydration of H_2O, in the temperature ranges relevant for subsea application.

In Figure 3 it seen that the CPA model over-predicts the experimental, with an AARD = 8.6% (See Table S3 in the Supporting Information). It is noteworthy that for both isobars, the model error increases with temperature.

The results for MEG in gas (y_{MEG}) are presented in Figure 4.

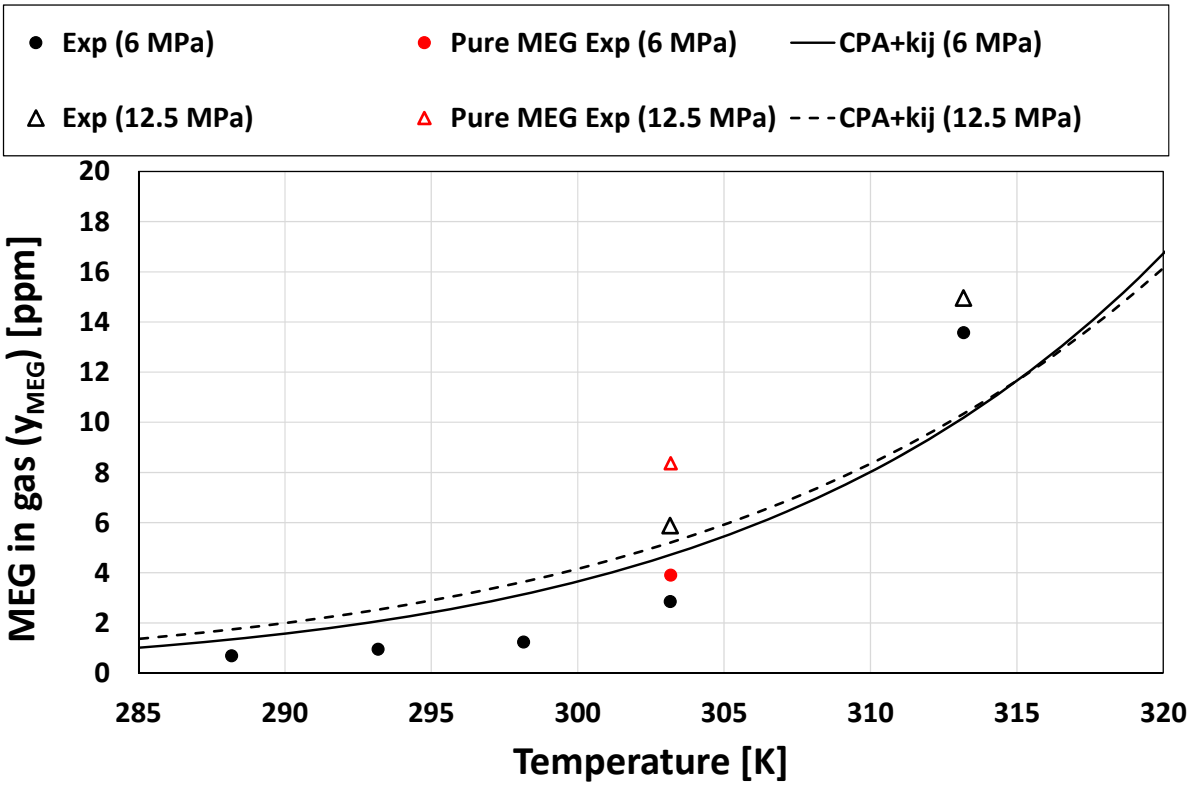

Figure 4. Experimental vapor phase MEG content in a mixture with water and natural gas components at T = (288-323) K, p = (6, 12.5) MPa and MEG feed purity of w_{MEG} = (90, >99.8) %.

For the 6.0 MPa isobar, the data follows an exponential trend from approximately 1 ppm to 14 ppm and y_{MEG} increases with both temperature and pressure. The change from the 90 wt% MEG to pure MEG results in an approximately one-third increase of y_{MEG} at 303 K. The

relative standard deviation is calculated at 3%, meaning that experimental uncertainty is estimated at ± 9% for a 0.997 confidence level.

The CPA model provides a qualitative description of the data, although a large error (~60%) is observed. The 6.0 MPa isobar is significantly over-predicted, which also occurred to a lesser degree (~12%) for ternary MEG-H_2O-C_1 systems. The modeling errors are given in Table S3 in the Supporting Information.

From the study of Boesen et al.[29] it was observed that both CPA and SRK-HV provided good predictions for y_{MEG} and y_{H2O} for MEG-H_2O-C_1-C_3 system measured by Ng and Chen.[22] However, when C_3 was substituted with CO_2 (modeled a solvating compound in CPA), both models severely under predicted the y_{MEG} data in the order of 50%. This indicates that the substitution/addition of CO_2 strongly affects both the experimental value and thermodynamic modeling prediction of y_{MEG}. It is noted that these data were measured for significantly different feed compositions and modeled using different parameters. However, we find a similar deviation in the predictive capability for y_{MEG} when comparing the data in this work (containing CO_2) to the ternary data (without CO_2) that we measured previously. From a modeling perspective, this is all the more interesting when considering that Boesen et al. showed that both models could represent both phases of the MEG-CO_2 binary data relatively well. It is noted that their binary prediction of y_{MEG} showed the greatest deviations at lower temperatures and pressures, which also occurs in this work.

DISCUSSION: PRIMARY NATURAL GAS COMPONENTS

The experimental data and CPA modeling results for the total dissolved natural gas are shown in Figure 5, where it is observed that only a weak temperature dependence exists for the range of our study. The effects of pressure and MEG purity are considerably more noticeable, as the amount of dissolved natural gas decreases by ~ 40% when the pressure is decreased from 12.5 to 6.0 MPa. Changing from aqueous MEG to pure MEG results in an approximately two-thirds increase of dissolved gas. CPA provides a relatively good description of the dissolved natural gas, yielding an over-prediction with an average value of 6% for all data points.

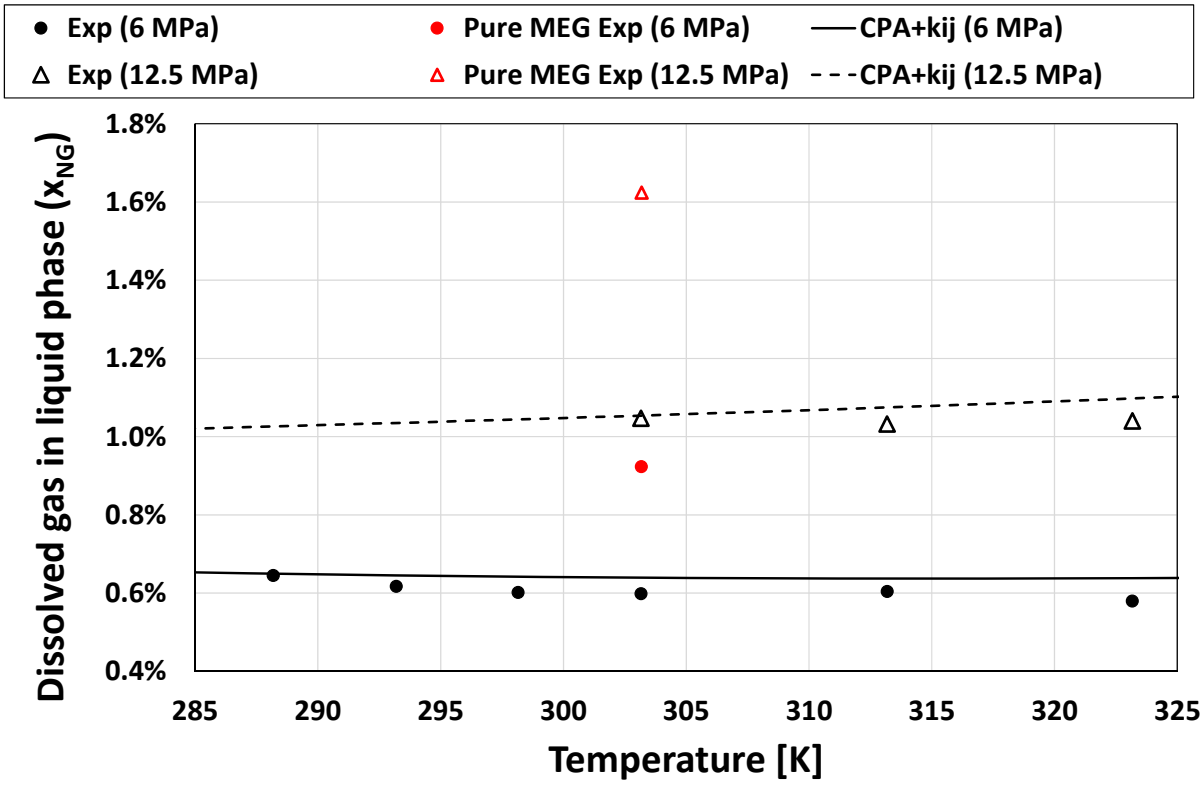

Figure 5. Experimental liquid phase content of total dissolved natural gas (x_{NG}) at T = (288-323) K, p = (6, 12.5) MPa and MEG feed purity of w_{MEG} = (90, >99.8) %.

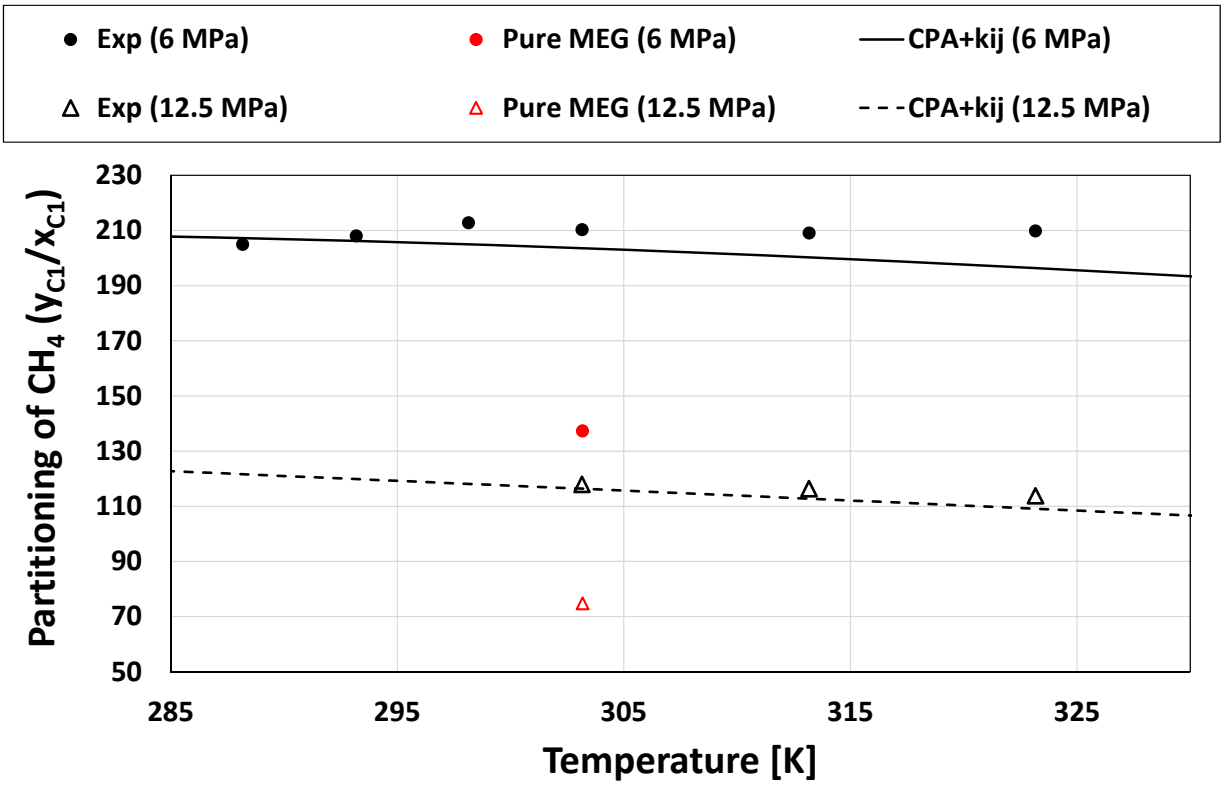

Figure 6. Experimental partition coefficients of methane (y_{C1}/x_{C1}) at T = (288-323) K, p = (6, 12.5) MPa and MEG feed purity of w_{MEG} = (90, >99.8) %.

The partition coefficient data and CPA modeling for selected natural gas components are shown in Figures 6-8. For C_1 and C_2, the partition coefficients are generally under-predicted by CPA due to the over-prediction of the amount of gas which dissolves into the liquid phase (x_i). There is not such a general trend from predictions of C_{2+} components. However, the overall modeling performance is quite satisfactory for most components as is evidenced by Figures 5-7 and the model errors presented in Tables S4-S5. Average overall modeling errors of less than 10% are reported for C_1-C_3, while trace components C_{3+} show errors in the range of ~50-60%. The notable exception is the dissolved fraction of isobutane (iC_4) for which errors are in the order of 300%. The large error is solely due to the lack of an appropriate binary interaction parameter. Although the newly regressed k_{ij} did somewhat improve the model prediction, it was found that a much larger interaction parameter (~0.15) would be

required to provide an accurate description of the data. Given that all MEG-C_{3+} interaction parameters have been fitted to Henry's constant or infinite dilution activity coefficient data, we would expect a marked improvement for the model performance if binary VLE data were available for these systems.

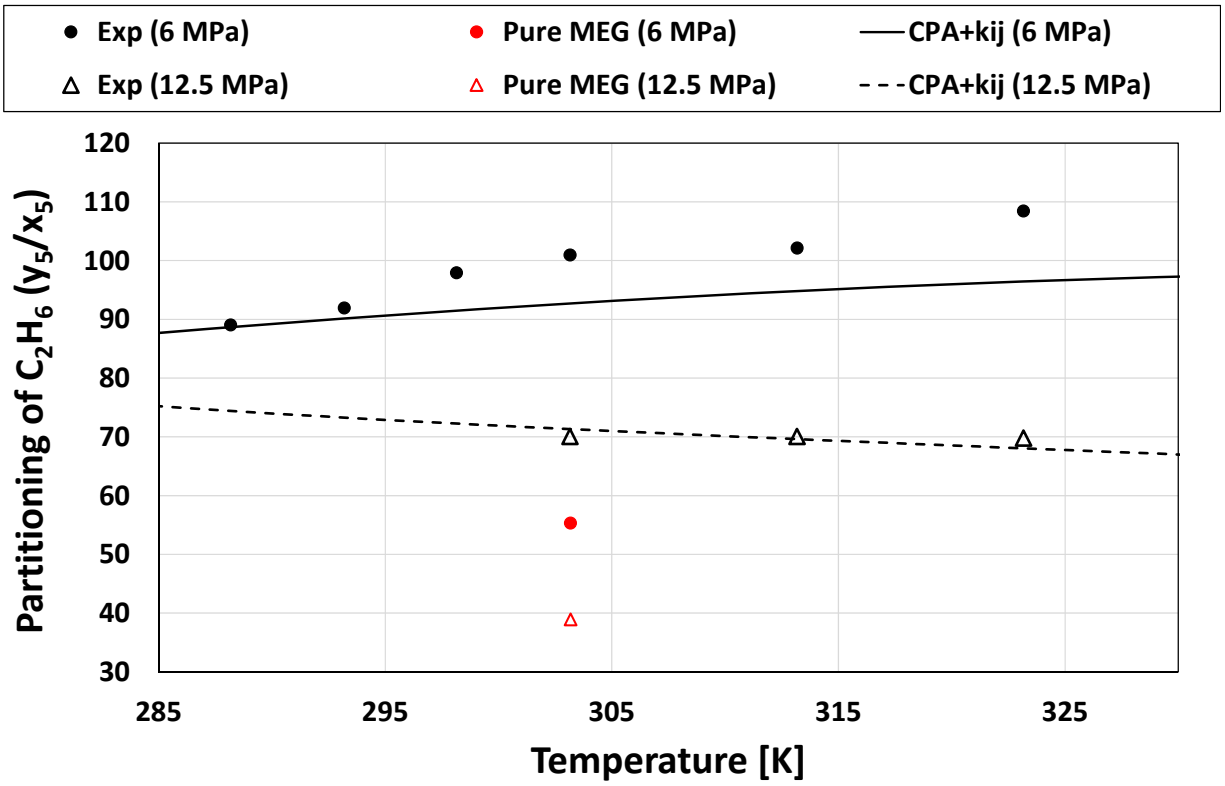

Figure 7. Experimental partition coefficients of ($y_{C2}x_{C2}$) at T = (288-323) K, p = (6, 12.5) MPa and MEG feed purity of w_{MEG} = (90, >99.8) %.

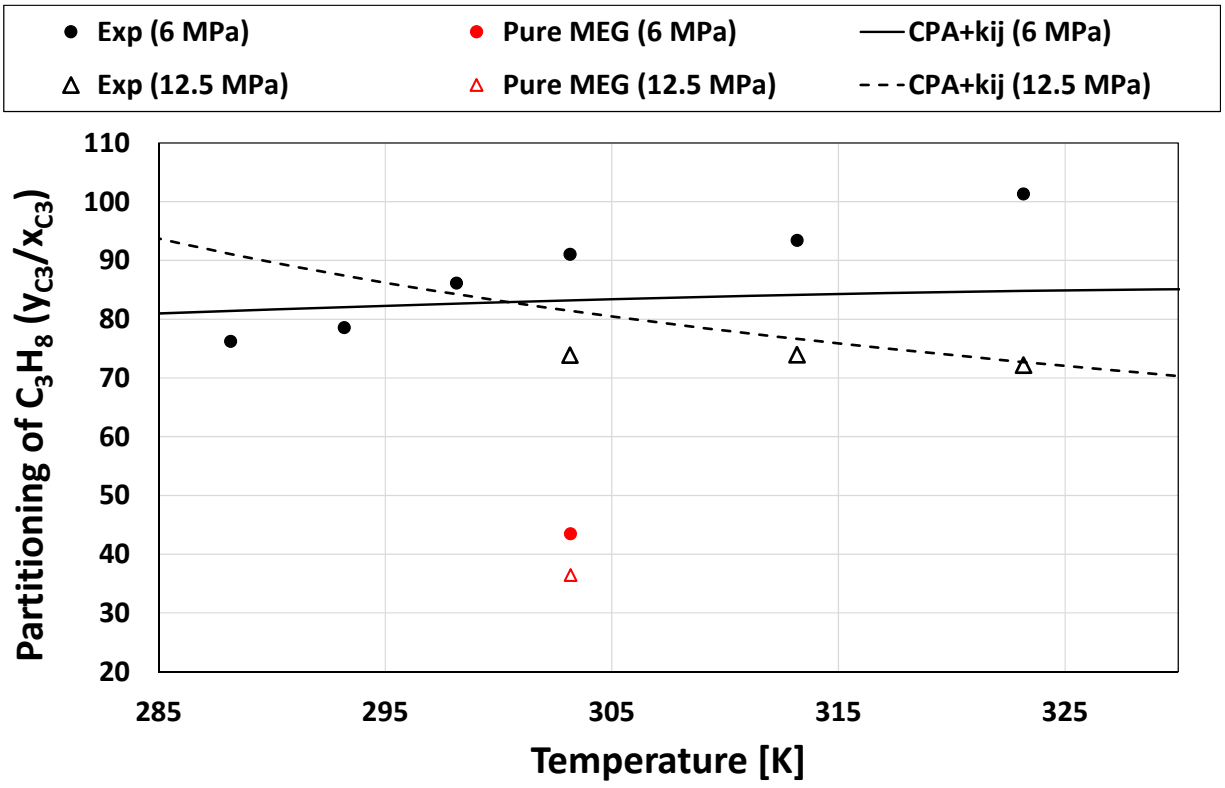

Figure 8. Experimental partition coefficients of propane (y_{C3}/x_{C3}) at T = (288-323) K, p = (6, 12.5) MPa and MEG feed purity of w_{MEG} = (90, >99.8) %.

For C_{1+} components, it is interesting to note that both the model prediction and experimental y_i/x_i data exhibit different temperature gradients (with one being positive, and the other negative) depending on the experimental pressure. This pressure dependence could be leveraged in certain separation and processing applications.

DISCUSSION: INERT COMPONENTS

For the discussion inert (i.e. non-hydrocarbon) compounds, the effect of CO_2 has been found to be most important. With the partition coefficients shown in Figure 9, it is again seen that CPA slightly under-predicts y_i/x_i for gasses due to an over-prediction of x_i. For the case of CO_2, the prediction errors are of a similar magnitude to those for C_1-C_3 with an average of 14% for x_i and 10% for y_i/x_i.

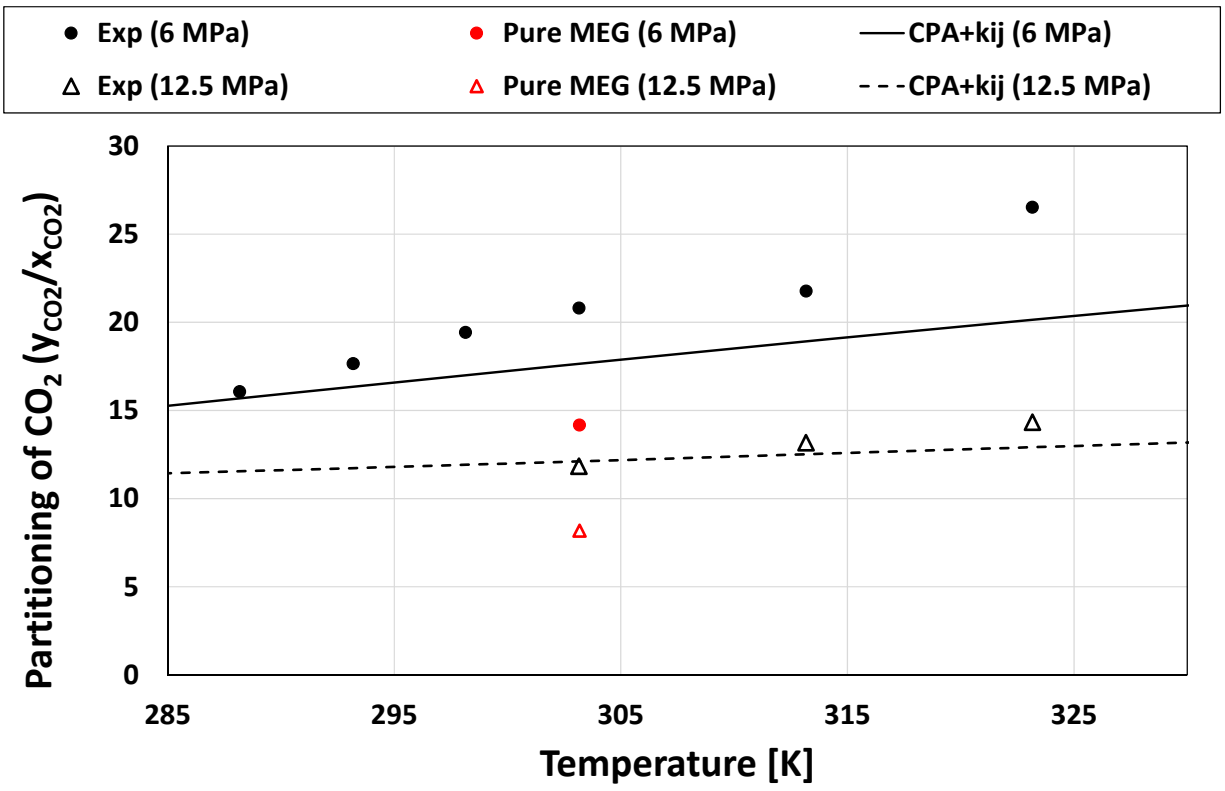

Figure 9. Experimental partition coefficients of carbon dioxide ($y_{CO2}x_{CO2}$) at T = (288-323) K, p = (6, 12.5) MPa and MEG feed purity of w_{MEG} = (90, >99.8) %.

The results for N_2 are somewhat inconsistent, which is attributed to the relatively low content in the liquid phase and the additional processing step required for the data generation discussed in the experimental section. General trends are still evident, such the positive gradient of x_{N2} vs T.

CONCLUSIONS

11 new VLE experimental data points have been measured for a 20-component glycol-water-natural gas mixture. In order to evaluate temperature, pressure and glycol purity effects for the proposed high pressure subsea natural gas dehydration units, measurements were made at T = (288-323) K, p = (6.0, 12.5) MPa and $w_{MEG,feed}$ = (90, >99.8) %. MEG, water, carbon dioxide, nitrogen and natural gas compounds (methane to *n*- and *i*-pentane) phase distributions have been quantified using a combination of Karl Fischer titration, gas chromatography, mass spectrometry and density measurements. The experimental uncertainty is strongly related to concentration of the respective component with a range of u_r = (3-42) % calculated at a confidence level of 0.997. The lowest uncertainty was found for y_{H2O} and x_{C1} while the highest uncertainties occurred for trace components, such as y_{MEG} and x_{iC5} in the vapor and liquid phases respectively.

In natural gas dehydration, glycol acts as a stripping agent by removing water from the vapor phase. The water and glycol content of the vapor (product) phase are critical specifications for the design of dehydration facilities. From the experimental data it can be seen that y_{H2O} and y_{MEG} both increase exponentially with temperature, but have opposite reactions to changes in pressure. From comparisons with ternary data it is seen that the additional natural gas components have a very small effect on the water removal at temperatures appropriate for subsea operations. The data shows that the processing pressure determines the gradient of x_i versus T, especially for C_{1+} components, which should be considered for the design of the glycol regeneration unit.

The experimental results are compared to the CPA equation of state. CPA slightly over-predicts the water content of the vapor phase, with relatively small errors (~10%) especially at low temperatures (T < 300 K). For the prediction of y_{MEG} quite significant over-predictions

(~65%) were observed, which did not occur for the ternary MEG-H_2O-C_1 systems. These deviations are attributed to presence of CO_2 in the mixture, since similar modeling difficulties were also observed for other cases where CO_2 was added/substituted. Previously it has been shown that CPA over-predicts the fraction of dissolved methane for ternary MEG-H_2O-C_1 systems at similar experimental conditions. The same over-prediction was observed for C_1 and C_2 measured in this study leading to an under-prediction of the partition coefficients. No such general trends were observed for C_{2+} components, but the overall modeling performance was quite satisfactory. Average overall modeling errors were generally below 10-15% for major compounds, while modeling errors for trace compounds increased to around 60%. These errors could be decreased if sufficient binary VLE data were available for MEG-hydrocarbon systems.

From a design perspective it is seen that the proposed high pressure operation provided significantly improved dehydration capability. An increase in operating pressure from 6.0 MPa to 12.5 MPa leads to an approximately 30% decrease of the water content of the product stream. Lower temperatures and high glycol purity are also advantageous. Although CPA does over-predict several critical process parameters, the model generally provides a conservative result. For instance, the over-prediction of the water vapor content of the product stream means that a process designed on this basis should always operate within specification. Similarly, the over-prediction of dissolved natural gas means the glycol regeneration will be adequately designed to remove those compounds.

NOMENCLATURE

List of Symbols

Symbol	Description	Units
a_0	attractive energy parameter	$Pa \cdot m^6 \cdot mol^{-2}$
b	co-volume	$cm^3 \cdot mol^{-1}$
c_1	attractive energy temperature-correction	-
CI	confidence interval multiplier	-
CD	calibration deviation	%
g	radial distribution function	-
ID	inner diameter (of GC column)	μm
k_{ij}	binary interaction parameter	-
L	length (of GC column)	m
M	molar mass	$g \cdot mol^{-1}$
m	mass	g
n	number of moles	mol
p	pressure	MPa
R	universal gas constant = 8.314	$J \cdot mol^{-1} \cdot K^{-1}$
T	temperature	K
V	volume	mL

V_m	molar volume	$L \cdot mol^{-1}$
w_i	mass fraction of component i	$g \cdot g^{-1}$
x_i	liquid mole fraction of component I	$mol \cdot mol^{-1}$
y_i	vapor mole fraction of component i	$mol \cdot mol^{-1}$
z_i	molar feed fraction of component i	$mol \cdot mol^{-1}$
β	volume of association	-
ε/R	reduced association energy	K
Γ	reduced attractive energy parameter = $a_0/(b \cdot R)$	K
σ_x	standard deviation of data x	-
ρ	density	$g \cdot cm^{-3}$
ρ_m	molar density	$mol \cdot L^{-1}$
μ_x	mean value / average of data x	units of x

Abbreviations

AARD	average absolute relative deviation
AI	analyzer indicator
ARD	absolute relative deviation
assoc	association - with respect to intermolecular forces
ATD	auto thermal desorption

CPA	Cubic-Plus-Association equation of state
cy	cyclo (chemical ring structure)
DM	di-methyl (chemical group)
ea.	electron acceptor (negative association site)
ECR	Elliot combining rule
ed.	electron donor (positive association site)
FI	flow indicator
GC-MS	gas chromatography – mass spectrometry
HV	Huron-Vidal mixing rule
KF	Karl Fischer (titration method)
M	methyl (chemical group)
mCR-1	modified CR-1 combining rule
MEG	Mono-ethylene glycol / ethylene glycol / 1,2-ethanediol
NG	natural gas (refers to the compounds loaded from the gas cylinder)
NGD	natural gas dehydration
OF_{min}	objective function used in minimization procedure
PC	pressure controller
PI	pressure indicator
PT	pressure transmitter

SAFT	Statistical Associating Fluid Theory equation of state
sat	saturation (in reference to pure component density or vapor pressure)
SRK	Soave-Redlich-Kwong equation of state
TA	thermal adsorption
TC	temperature controller
TCD	thermal conductivity detector (used in GC analysis)
TI	temperature indicator
TT	temperature transmitter
VLE	Vapor-liquid equilibrium
μGC	micro gas chromatograph

ASSOCIATED CONTENT

Supporting Information

Experimental uncertainties for y_i, x_i, and y_i/x_i expressed as a percentage relative standard deviation (Tables S1-S2). CPA modeling errors for the experimental data expressed as percentage average absolute relative deviation (Tables S3-S5).

AUTHOR INFORMATION

Corresponding Author

Nicolas von Solms E-mail: nvs@kt.dtu.dk

Author Contributions

The manuscript was written through contributions of all authors. All authors have given approval to the final version of the manuscript.

Acknowledgment

The authors gratefully acknowledge the financial support and permission to publish the data from Equinor (formerly Statoil A/S, Norway) within the framework of the joint industry project: 'Chemicals in Gas Processing'. The authors also wish to thank Marie Vikre Danielsen, Ole Johan Berg, Gunn Iren Rudolfsen and Kaja Klæbo Hjelseth for their assistance with various aspects of the experimental work.

REFERENCES

(1) Løkken, T. V. Water Vapour Measurements in Natural Gas in the Presence of Ethylene Glycol. *J. Nat. Gas Sci. Eng.* **2013**, *12*, 13–21.

(2) Scholes, C. A.; Stevens, G. W.; Kentish, S. E. Membrane Gas Separation Applications in Natural Gas Processing. *Fuel* **2012**, *96*, 15–28.

(3) Dalane, K.; Dai, Z.; Mogseth, G.; Hillestad, M.; Deng, L. Potential Applications of Membrane Separation for Subsea Natural Gas Processing: A Review. *J. Nat. Gas Sci. Eng.* **2017**, *39*, 101–117.

(4) Lin, H.; Thompson, S. M.; Serbanescu-Martin, A.; Wijmans, J. G.; Amo, K. D.; Lokhandwala, K. A.; Merkel, T. C. Dehydration of Natural Gas Using Membranes. Part I: Composite Membranes. *J. Membr. Sci.* **2012**, *413–414*, 70–81.

(5) Gandhidasan, P.; Al-Farayedhi, A. A.; Al-Mubarak, A. A. Dehydration of Natural Gas Using Solid Desiccants. *Energy* **2001**, *26*, 855–868.

(6) Farag, H. A. A.; Ezzat, M. M.; Amer, H.; Nashed, A. W. Natural Gas Dehydration by Desiccant Materials. *Alex. Eng. J.* **2011**, *50*, 431–439.

(7) Santos, M. G. R. S.; Correia, L. M. S.; de Medeiros, J. L.; Araújo, O. de Q. F. Natural Gas Dehydration by Molecular Sieve in Offshore Plants: Impact of Increasing Carbon Dioxide Content. *Energy Convers. Manag.* **2017**, *149*, 760–773.

(8) Yu, G.; Dai, C.; Wu, L.; Lei, Z. Natural Gas Dehydration with Ionic Liquids. *Energy Fuels* **2017**, *31*, 1429–1439.

(9) Wen, C.; Cao, X.; Yang, Y. Swirling Flow of Natural Gas in Supersonic Separators. *Chem. Eng. Process. Process Intensif.* **2011**, *50*, 644–649.

(10) Parks, D.; Amin, R. Novel Subsea Gas Dehydration Process, the Process Plant and Dehydration Performance. *J. Pet. Sci. Eng.* **2012**, *81*, 94–99.

(11) Parks, D.; Pack, D. Design Concept for Implementation of a Novel Subsea Gas Dehydration Process for a Gas/Condensate Well. *J. Pet. Sci. Eng.* **2013**, *109*, 18–25.

(12) Díaz, R.; Jiménez-Junca, C.; Roa, D. A Novel Absorption Process for Small-Scale Natural Gas Dew Point Control and Dehydration. *J. Nat. Gas Sci. Eng.* **2016**, *29*, 264–274.

(13) Fredheim, A. O.; Johnsen, C. G.; Johannessen, E.; Kojen, G. P. Gas-2-Pipe™, A Concept for Treating Gas to Rich Gas Quality in a Subsea or Unmanned Facility. Annu. Offshore Technol. Conf., Proc., Houston, **2016**.

(14) Jou, F. Y.; Otto, F. D.; Mather, A. E. Solubility of Methane in Glycols at Elevated Pressures. *Can. J. Chem. Eng.* **1994**, *72*, 130–133.

(15) Zheng, D.-Q.; Ma, W.-D.; Wei, R.; Guo, T.-M. Solubility Study of Methane, Carbon Dioxide and Nitrogen in Ethylene Glycol at Elevated Temperatures and Pressures. *Fluid Phase Equilib.* **1999**, *155*, 277–286.

(16) Wang, L.-K.; Chen, G.-J.; Han, G.-H.; Guo, X.-Q.; Guo, T.-M. Experimental Study on the Solubility of Natural Gas Components in Water with or without Hydrate Inhibitor. *Fluid Phase Equilib.* **2003**, *207*, 143–154.

(17) Jou, F.-Y.; Schmidt, K. A. G.; Mather, A. E. Vapor–liquid Equilibrium in the System Ethane+ethylene Glycol. *Fluid Phase Equilib.* **2006**, *240*, 220–223.

(18) Folas, G. K.; Berg, O. J.; Solbraa, E.; Fredheim, A. O.; Kontogeorgis, G. M.; Michelsen, M. L.; Stenby, E. H. High-Pressure Vapor–liquid Equilibria of Systems Containing Ethylene Glycol, Water and Methane: Experimental Measurements and Modeling. *Fluid Phase Equilib.* **2007**, *251*, 52–58.

(19) Abdi, M. A.; Hussain, A.; Hawboldt, K.; Beronich, E. Experimental Study of Solubility of Natural Gas Components in Aqueous Solutions of Ethylene Glycol at Low-Temperature and High-Pressure Conditions. *J. Chem. Eng. Data* **2007**, *52*, 1741–1746.

(20) Galvão, A. C.; Francesconi, A. Z. Solubility of Methane and Carbon Dioxide in Ethylene Glycol at Pressures up to 14 MPa and Temperatures Ranging from (303 to 423) K. *J. Chem. Thermodyn.* **2010**, *42*, 684–688.

(21) Kruger, F. J.; Danielsen, M. V.; Kontogeorgis, G. M.; Solbraa, E.; von Solms, N. Ternary Vapor–Liquid Equilibrium Measurements and Modeling of Ethylene Glycol (1) + Water (2) + Methane (3) Systems at 6 and 12.5 MPa. *J. Chem. Eng. Data* **2018**, *63*, 1789–1796.

(22) Ng, H.-J.; Chen, C.-J. Research Report RR-149: Vapour−Liquid and Vapour−Liquid−Liquid Equilibria for H_2S, CO_2, Selected Light Hydrocarbons and a Gas Condensate in Aqueous Methanol or Ethylene Glycol Solutions. Gas Processors' Association (GPA) 1995.

(23) Soave, G. Equilibrium Constants from a Modified Redlich-Kwong Equation of State. *Chem. Eng. Sci.* **1972**, *27*, 1197–1203.

(24) Peng, D.-Y.; Robinson, D. B. A New Two-Constant Equation of State. *Ind. Eng. Chem. Fundam.* **1976**, *15*, 59–64.

(25) Chapman, W. G.; Gubbins, K. E.; Jackson, G.; Radosz, M. SAFT: Equation-of-State Solution Model for Associating Fluids. *Fluid Phase Equilib.* **1989**, *52*, 31–38.

(26) Chapman, W. G.; Gubbins, K. E.; Jackson, G.; Radosz, M. New Reference Equation of State for Associating Liquids. *Ind. Eng. Chem. Res.* **1990**, *29*, 1709–1721.

(27) Huang, S. H.; Radosz, M. Equation of State for Small, Large, Polydisperse, and Associating Molecules. *Ind. Eng. Chem. Res.* **1990**, *29*, 2284–2294.

(28) Kontogeorgis, G. M.; Voutsas, E. C.; Yakoumis, I. V.; Tassios, D. P. An Equation of State for Associating Fluids. *Ind. Eng. Chem. Res.* **1996**, *35*, 4310–4318.

(29) Boesen, R. R.; Herslund, P. J.; Sørensen, H. Loss of Monoethylene Glycol to CO_2- and H_2S-Rich Fluids: Modeled Using Soave–Redlich–Kwong with the Huron and Vidal

Mixing Rule and Cubic-Plus-Association Equations of State. *Energy Fuels* **2017**, *31*, 3417–3426.

(30) Liang, X.; Aloupis, G.; Kontogeorgis, G. M. Data Requirements and Modeling for Gas Hydrate-Related Mixtures and a Comparison of Two Association Models. *J. Chem. Eng. Data* **2017**, *62*, 2592–2605.

(31) Kontogeorgis, G. M.; V. Yakoumis, I.; Meijer, H.; Hendriks, E.; Moorwood, T. Multicomponent Phase Equilibrium Calculations for Water–methanol–alkane Mixtures. *Fluid Phase Equilib.* **1999**, *158–160*, 201–209.

(32) Kontogeorgis, G. M.; Folas, G. K. Chapter 9: The Cubic-Plus-Association Equation of State. In *Thermodynamic Models for Industrial Applications*; John Wiley & Sons, Ltd, 2010; pp 261–297.

(33) Kontogeorgis, G. M.; Folas, G. K.; Muro-Suñé, N.; von, S.; Michelsen, M. L.; Stenby, E. H. Modelling of Associating Mixtures for Applications in the Oil & Gas and Chemical Industries. *Fluid Phase Equilib.* **2007**, *261*, 205–211.

(34) Kontogeorgis, G. M.; Michelsen, M. L.; Folas, G. K.; Derawi, S.; von Solms, N.; Stenby, E. H. Ten Years with the CPA (Cubic-Plus-Association) Equation of State. Part 1. Pure Compounds and Self-Associating Systems. *Ind. Eng. Chem. Res.* **2006**, *45*, 4855–4868.

(35) Kontogeorgis, G. M.; Michelsen, M. L.; Folas, G. K.; Derawi, S.; von Solms, N.; Stenby, E. H. Ten Years with the CPA (Cubic-Plus-Association) Equation of State. Part 2. Cross-Associating and Multicomponent Systems. *Ind. Eng. Chem. Res.* **2006**, *45*, 4869–4878.

(36) Kontogeorgis, G. M. Association Theories for Complex Thermodynamics. *Chem. Eng. Res. Des.* **2013**, *91*, 1840–1858.

(37) Kruger, F.; Kontogeorgis, G. M.; von Solms, N. New Association Schemes for Mono-Ethylene Glycol: Cubic-Plus-Association Parameterization and Uncertainty Analysis. *Fluid Phase Equilib.* **2018**, *458*, 211–233.

(38) Tsivintzelis, I.; Kontogeorgis, G. M.; Michelsen, M. L.; Stenby, E. H. Modeling Phase Equilibria for Acid Gas Mixtures Using the CPA Equation of State. I. Mixtures with H_2S. *AIChE J.* **2010**, *56*, 2965–2982.

(39) Tsivintzelis, I.; Kontogeorgis, G. M.; Michelsen, M. L.; Stenby, E. H. Modeling Phase Equilibria for Acid Gas Mixtures Using the CPA Equation of State. Part II: Binary Mixtures with CO_2. *Fluid Phase Equilib.* **2011**, *306*, 38–56.

(40) Tsivintzelis, I.; Ali, S.; Kontogeorgis, G. M. Modeling Phase Equilibria for Acid Gas Mixtures Using the Cubic-Plus-Association Equation of State. 3. Applications Relevant to Liquid or Supercritical CO_2 Transport. *J. Chem. Eng. Data* **2014**, *59*, 2955–2972.

(41) Tsivintzelis, I.; Ali, S.; Kontogeorgis, G. M. Modeling Phase Equilibria for Acid Gas Mixtures Using the CPA Equation of State. Part IV. Applications to Mixtures of CO_2 with Alkanes. *Fluid Phase Equilib.* **2015**, *397*, 1–17.

(42) Tsivintzelis, I.; Kontogeorgis, G. M. Modelling Phase Equilibria for Acid Gas Mixtures Using the CPA Equation of State. Part V: Multicomponent Mixtures Containing CO_2 and Alcohols. *J. Supercrit. Fluids* **2015**, *104*, 29–39.

(43) Tsivintzelis, I.; Kontogeorgis, G. M. Modelling Phase Equilibria for Acid Gas Mixtures Using the CPA Equation of State. Part VI. Multicomponent Mixtures with Glycols Relevant to Oil and Gas and to Liquid or Supercritical CO_2 Transport Applications. *J. Chem. Thermodyn.* **2016**, *93*, 305–319.

(44) Perfetti, E.; Thiery, R.; Dubessy, J. Equation of State Taking into Account Dipolar Interactions and Association by Hydrogen Bonding: II—Modelling Liquid–vapour Equilibria in the H_2O–H_2S, H_2O–CH_4 AND H_2O–CO_2 Systems. *Chem. Geol.* **2008**, *251*, 50–57.

(45) Bjørner, M. G.; Sin, G.; Kontogeorgis, G. M. Uncertainty Analysis of the CPA and a Quadrupolar CPA Equation of State – With Emphasis on CO_2. *Fluid Phase Equilib.* **2016**, *414*, 29–47.

(46) Derawi, S. O.; Michelsen, M. L.; Kontogeorgis, G. M.; Stenby, E. H. Application of the CPA Equation of State to Glycol/Hydrocarbons Liquid–liquid Equilibria. *Fluid Phase Equilib.* **2003**, *209*, 163–184.

(47) Yakoumis, I. V.; Kontogeorgis, G. M.; Voutsas, E. C.; Tassios, D. P. Vapor-Liquid Equilibria for Alcohol/Hydrocarbon Systems Using the CPA Equation of State. *Fluid Phase Equilib.* **1997**, *130*, 31–47.

(48) Awan, J. A.; Tsivintzelis, I.; Breil, M. P.; Coquelet, C.; Richon, D.; Kontogeorgis, G. M. Phase Equilibria of Mixtures Containing Organic Sulfur Species (OSS) and Water/Hydrocarbons: VLE Measurements and Modeling Using the Cubic-Plus-Association Equation of State. *Ind. Eng. Chem. Res.* **2010**, *49*, 12718–12725.

(49) Brigham Young University (BYU). *DIADEM Professional - DIPPR Information and Data Evaluation Manager*; 2016.

(50) Folas, G. K.; Kontogeorgis, G. M.; Michelsen, M. L.; Stenby, E. H. Application of the Cubic-Plus-Association (CPA) Equation of State to Complex Mixtures with Aromatic Hydrocarbons. *Ind. Eng. Chem. Res.* **2006**, *45*, 1527–1538.

(51) Ioannis Tsvintzelis; Bjørn Maribo-Mogensen. *The Cubic-Plus-Association EoS: Parameters for Pure Compounds and Interaction Parameters*; Technical Report; DTU-CERE, 2012.

(52) Afzal, W.; Breil, M. P.; Théveneau, P.; Mohammadi, A. H.; Kontogeorgis, G. M.; Richon, D. Phase Equilibria of Mixtures Containing Glycol and N-Alkane: Experimental Study of Infinite Dilution Activity Coefficients and Modeling Using the Cubic-Plus-Association Equation of State. *Ind. Eng. Chem. Res.* **2009**, *48*, 11202–11210.

(53) Folas, G. Modeling of Complex Mixtures Containing Hydrogen Bonding Molecules. PhD, Technical University of Denmark (DTU): Kongens Lyngby, 2007.

(54) Renon, H.; Lenoir, J. Y.; Renault, P. Gas Chromatographic Determination of Henry's Constants of 12 Gases in 19 Solvents. *J. Chem. Eng. Data* **1971**, *16*, 340–342.